MICROSTRUCTURE INVESTIGATION OF CAST IRONS WITH NODULAR AND FLAKE GRAPHITE VIA NANOINDENTATION

Peter Petruš – Igor Barényi* – Jozef Majerík

Department of mechanical technologies and materials, Faculty of special technology, Alexander Dubcek University of Trencin, Ku kyselke 469, Trencin, Slovakia
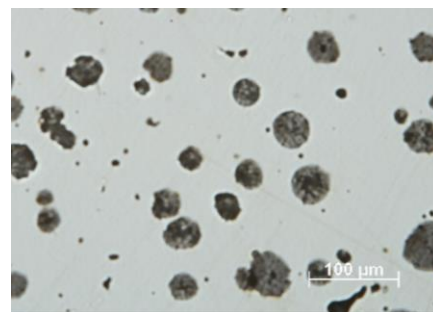
ARTICLE INFO	Abstract
	The paper investigates and compares the local mechanical properties of microstructure components in grey iron EN GJL -300 and ductile iron EN GJS -500-7. The microstructure of both cast irons is analysed by LOM, and then certain microstructure components found and their local mechanical properties are investigated. Finally, the resulting nanohardness and reduced Young modulus of the components are discussed and compared between the two cast irons used. A Hysitron TI -950 gauge with Triboscan software is used to perform experiment measurements.

1 Introduction

The basic types of graphitic cast iron cannot be distinguished or classified by chemical composition as steels can. All cast irons generally have a high carbon and silicon content. The most important criterion for their classification is the shape of the graphite. Their mechanical properties also vary depending on the graphite form. Basic graphite forms include flaky, spherical (nodular), and compacted graphite. Intermediate forms such as coral graphite, explosive graphite, etc. can also be found [1], [2]. The best known type of cast iron is grey iron, in which the flake-like shape of the graphite (Figure 1a) concentrates stresses and promotes cracking, making it less ductile and strong. However, grey iron can be improved during the metallurgical process of its production by adding a nodular iron casting agent, which is usually magnesium or, less commonly, cerium, tellurium, or yttrium [3]. The nodular graphite agent allows the graphite to solidify into spherical particles known as nodular iron, resulting in ductile iron (Figure 1b). This form of graphite provides better mechanical properties of the cast iron and prevents the formation of cracks, which earns the alloy the name ductile iron [4], [5].

a) flake-like graphite   *b) spheroidal graphite*

Figure 1. Graphite shape for grey cast iron (a) and ductile iron (b).

* Corresponding author
E-mail address: igor.barenyi@tnuni.sk

The morphology and distribution of the microstructural phases in cast irons were studied by several authors [6] - [8]. More multiscale and micromechanical models are now emerging in this regard [9] – [11], but the major challenge associated with developing the models is the lack of knowledge concerning the mechanical behavior of the individual constituents forming the microstructure of cast irons. That is why this paper aims to map and then compare the local mechanical properties of microstructure constituents present in grey cast iron and ductile iron. An important factor affecting the resulting mechanical properties of the cast iron is also the matrix surrounding graphitic particles. The matrix of both grey cast iron and ductile iron can range from ferrite to pearlite and various combinations of the two phases. Moreover, the matrix can be heat treated to obtain bainitic or martensitic structures with higher strength.

2   Material and methods

2.1 Materials used for experiment

Two cast irons with different graphite shapes were used for the experiments. The first is grey cast iron EN GJL 500 with flaky graphite and the second is ductile cast iron EN GJS -500-7 with globulitic graphite. Both types of cast iron have a pearlitic matrix. The chemical composition of the test materials used, evaluated by the Spectrolab JrCCD emission spectrometer, is shown in Table 1. The basic mechanical properties obtained by standard tensile strength test and Brinell hardness test are listed in Table 2. The test specimens for all experiments performed were prepared from as-received materials without heat treatment.

Table 1. Chemical composition of used experimental materials (wt.%)

Element	EN GJL-300	EN GJS-500-7
C	3.11	3.62
Si	2.32	2.92
Mn	0.62	0.21
S	0.06	0.02
P	0.17	0.10
Others / Alloying	residual	residual
Fe	ballance	ballance

Table 2. Basic mechanical properties of used experimental materials

	R_m, MPa	R_e, MPa	Hardness, HB	Toughness (20°C), J/cm^2
EN GJL-300	290	218	205	5
EN GJS-500-7	492	322	235	8.5

Light microscopy analysis was performed to obtain more detailed information about the microstructure of both materials as an input to nanoindentation analysis. Samples for metallographic analysis were prepared using standard preparation steps as are grinding, polishing and finally etching in nital (3% solution of H_2NO_3 in ethanol). The microstructure of EN GJL-300 is shown in Figure 2. Black graphite flakes are clearly visible in the structure. It is also possible to recognize the pearlitic character of the matrix consisting of ferrite and cementite lamellas. The microstructure of EN GJS-500-7 is shown in Figure 3. As was stated above, this cast iron is characterized by typical black graphitic nodules with globulitic shapes. The nodules are surrounded by white ferritic rings. These regions are formed as a result of diffusion of carbon towards the graphitization centre leaving behind carbon depleted region, which transforms into a low-carbon phase (ferrite) [5]. Matrix is also pearlitic, but the distribution of ferrite and cementite within the pearlite is not regularly lamellar.
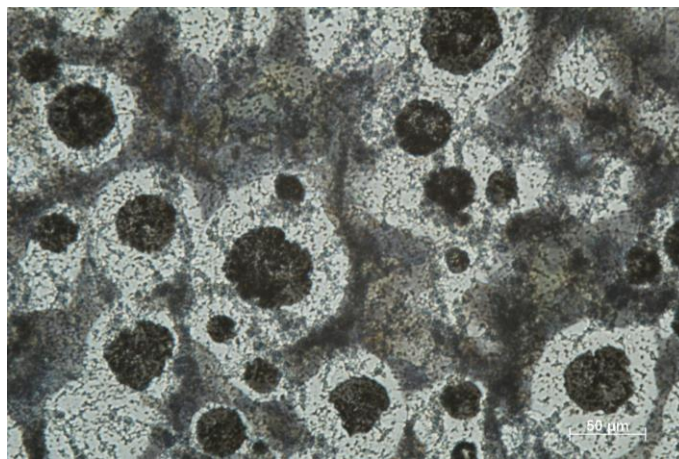
Figure 2. Microstructure of EN GJL-300.

Figure 3. Microstructure of EN GJS-500-7.

2.2 Quasistatic nanoindentation

Investigation of local mechanical properties of structural components present within the experimental material was performed by quasistatic nanoindentation based on Oliver & Pharr method [12]. The method is based on pushing a diamond-tipped indenter head into a material, but unlike conventional indentation methods for hardness measurement, a parameter of impress can not be used to evaluate the resulting value. This approach is impracticable in the range of nanometres. Oliver & Pharr's method uses the monitoring of the displacement (h) as a function of the load (F) during both load and unload cycles of the indentation process where the resulting relation F-h is called nanoindentation curve (Figure 4). Loading part of the curve is used to evaluate nanohardness H which is defined as the contact pressure under the indenter [13]:

$$H = \frac{F}{A_c}$$

(1)

where F is the load and A_c is the projected contact area calculated at a depth of indentation h. The unloading part is related to recovering elastic deformation and can be used to calculate the Young modulus of the material. The result indetation deep h_p corresponds with the retained plastic deformation of the material caused by nanoindetaton.
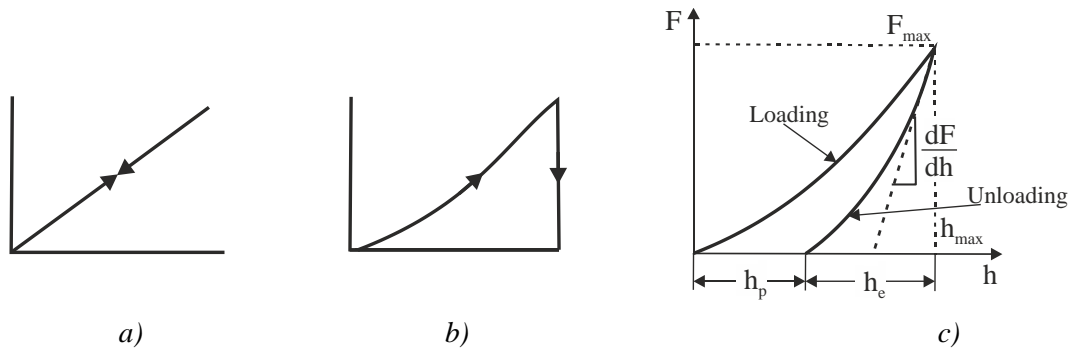
Figure 4. Nanoindentation curves: a – ideally elastic material, b – ideally plastic material, c – real material [12].

The initial slope (*S*) of the unloading curve can be related to the elastic modulus of the material using equation [12]:

$$S = \frac{dF}{dh} = \frac{2E_r\sqrt{A_c}}{\sqrt{\pi}} \tag{2}$$

where S is the initial slope of the unloading curve or contact stiffness, F is the applied load and E_r is the reduced Young modulus. Conventional Young modulus of the sample (E_s) can be related to the reduced modulus (E_r) using equation 3 provided the indenter modulus (E_i) and Poisson's ratios of the specimen and indenter (v_s and v_i respectively) are known or can be estimated. According to some authors [9, 10], the diamond indenter behaves rigidly and equation 3 can be reduced to equation 4 by omitting its second part related to indentor material properties.

$$\frac{1}{E_r} = \frac{1 - v_s^2}{E_s} + \frac{1 - v_i^2}{E_i} \tag{3}$$

$$\frac{1}{E_r} = \frac{1 - v_s^2}{E_s} \tag{4}$$

All presented quasi-static nanoindentation tests of the experimental samples were performed at room temperature using the Hysitron TI -950 measuring device equipped with the Triboscan software in the CEDITEK Laboratory of Mechanical Testing in Trencin (Faculty of Special Technology). The same samples prepared for optical microscopy were used for nanoindentation. The instrument has a built-in microscope objective, which can be used to display a LOM image of the examined surface at the selected location. This image was used together with the previously mentioned microstructural analysis of the test materials to select the area of indentation. The next step of the procedure is in-situ SPM (scanning probe microscopy) scanning of the selected area with a specific size. To produce images, the indenter tip oscillates over the surface at a specific frequency and a low load while scanning the selected area without causing physical changes to the material. In the final step, specific nanoindentation points are marked within the SPM scan where nanoindentation is then performed. A standard trapezoid was used as the loading curve for all nanoindentations performed.

The maximum loading force F=1000 µN at a penetration time of t=2 s was used due to the size of the particles and to avoid cracking during the process. Berkovich indenter geometry was used for nanoindentation analysis. With this geometry and indenter force, the maximum indentation depth varied in the range of 95 ÷ 200 nm and the indentation size in the rangeof 0.2 ÷ 0.6 µm2. These parameters are thus suitable to cover all measured areas of the investigated cast iron parts.

3   Results and discussion

SPM scan of area 10x10 µm obtained from the EN GJL 300 sample is shown in Figure. 5. The scan display part of graphite flake as well as pearlitic lamellas of ferrite and cementite. All these structure components were chosen as nanoindentation places (green points) where three measurements for every component were realized.
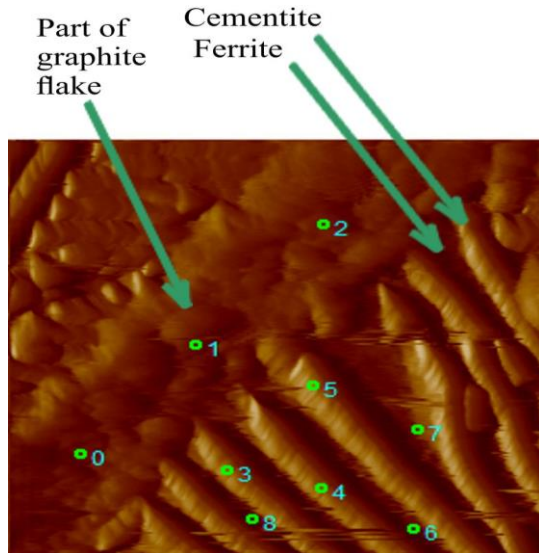

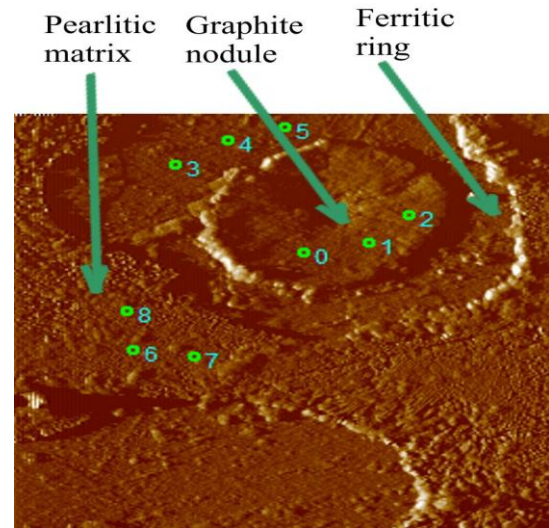*Figure 5. Nanoindentation point layout in SPM scan (10x10 µm) for EN GJL-300.*

Figure 6. Nanoindentation point layout in SPM scan (75x75 µm) for EN GJS-500-7.

A scanning area of 75x75 µm was chosen for scanning of the EN GJS-500-7 to capture the complete graphitic nodule and its ring. These structure components together with the matrix were then nanoindented in selected (green) points (Figure 6). Evaluated values of nanohardness H and reduced Young modulus E_r of structure components for EN GJL 300 cast iron are in Table 3 and for ductile iron EN GJS-500-7 in Table 4. In a case of EN GJL-300, all basic structure component is visible in SPM scan and the values of local mechanical properties correspond with identified components and their values are in ranges determined by other works [3], [5], [11]. Graphite flake has lowest hardness and reduced modulus with analogically highest resulting indentation depth. This show most favorable elastic-palstic properties of the grafite, compared to cementite lamella for example, which is hardest and more brittle (with higher E_r and lower h_p).

Table 3. Nanoindentation results for EN GJL-300.

Position	H, GPa	E_r, GPa	h_p, nm	Component	Average H	Average E_r
0	0.90	46.56	190.79	Graphite flake	0.95	43.98
1	0.99	40.84	188.29			
2	0.95	45.53	202.13			
3	4.64	152.16	87.06	Cementite lamella	4.52	165.72
4	4.50	179.35	90.95			
5	4.45	165.64	94.19			
6	1.64	127.06	170.27	Ferrite lamella	1.56	123.90
7	1.46	112.28	162.50			
8	1.58	132.36	171.93			

In the case of EN GJS-500-7, graphite nodule indicates higher nanohardness than graphite in form of flake for grey cast iron. Some authors [14] - [16] pointed out that, the graphite nodule can consist of complex oxides and sulfides of nodulizing elements, which serve as nucleation site during solidification with the result of the

spheroidal shape of the graphite. We assume that the presence of these oxides can also cause the increase of the hardness of the nodule. In addition to higher hardness, the nodule shows lower h_p, what means lower proportion of plastic deformation caused by indentation. As is known in general, graphite nodule causes higher strength of the iron. The combination of measured H and h_p is consistent with this fact.

Table 4. Nanoindentation results for EN GJS-500-7.

Position	H, GPa	E$_r$, GPa	h$_p$, nm	Component	Average H	Average E$_r$
0	1.23	39.39	175.99	Graphite nodule	1.31	37.93
1	1.13	33.54	183.11			
2	1.57	40.84	156.67			
3	3.14	192.25	133.78	Ferritic ring	2.59	193,98
4	2.69	209.20	143.24			
5	2.85	180.50	139.88			
6	2.23	143.09	152.90	Perlite mx. (F)		
7	5.53	177.66	84.62	Perlite mx. (Fe$_3$C)	4.86	177.14
8	4.19	176.62	111.73			

The measured reduced Young modulus of the nodule is slighty lower as the flake modulus but the difference is small. Moreover, some authors mentioned [5], [17], that the reduced modulus can softly vary depending on the indenter tip location within the nodula. Therefore, the values of both modules can be considered as approximately equal. Pearlite components of the matrix (ferrite and cementite) for EN GJS-500-7 could not be visually recognized even in a more detailed SPM scan (10x10 μm) of the matrix area. However, indent in position 6 and related measured values of H and E_r (in Table 4) corresponds with ferrite, while positions 7 and 8 correspond with cementite properties measured for grey cast iron (Table 3).

4   Conclusion

The paper describes the analysis of the microstructure and subsequently the local mechanical properties of microstructural constituents for grey cast iron EN GJL -300 and ductile cast iron EN GJS -500-7. The investigation focused primarily on the differences between the nanohardness and reduced elastic modulus of lamellar graphite and nodular graphite, but other microstructural constituents were also subjected to nanoindentation. The investigation can be summarised as follows:

1. Nanohardness of the graphite nodule shows a higher value than graphite flake. The cause may be the presence of nodulizing elements compounds within the nodule. However, higher nanohardness together with lower permanent plastic deformation (h_p value) of the nodule can be one of the factors of increased strength of the ductile cast iron in compare to gray cast iron.
2. The reduced Young modulus of the graphite nodule is almost equal as the graphite flake. However, the overall properties of gray or ductile cast depends not not only on the nanomechical properties of the individual phases. Morphology, distribution and proportion of the phases are also very important factors. From that point of view, cast iron can be considered as a composite material, where graphite and matrix are main constiutents.
3. Ferrite ring surrounding graphite nodule shows comparable hardness with other ferrite-based constituents of pearlite matrix but its Young modulus is higher. Further investigation of the possible presence of other compounds in the ring is needed.
4. Both investigated cast iron has pearlite matrix. The values of local mechanical properties of ferrite and cementite within the matrix show corresponding values when comparing both cast iron matrixes. Some differences are caused by the different chemical compositions of the cast irons.

The presented investigation is a part of larger research focused on increasing machinability and related quality parameters for the products made of cast irons.

_____

References

[1]   R. Ruxanda, D.M. Stefanescu, "Graphite shape characterization in cast iron – from visual estimate to fractal dimension", *International Journal of Cast Metals Research*, January 2002, doi: 10.1080/13640461.2002.11819439. *(Journal article)*

[2]   C. Fragassa, R. Zigulic, A. Pavlovic, "Push-pull fatigue tests on ductile and vermicular cast irons", *Engineering Review*, vol. 36, Issue 3, pp. 269-280, 2016, ISSN 13309587 *(Journal article)*

[3]   T. Andriollo, S. Fæsterb, G. Winthera, "Probing the structure and mechanical properties of the graphite nodules in ductile cast irons via nano-indentation", *Mechanics of Materials,* vol. 122 (2018), pp. 85–95, doi: 10.1016/j.mechmat.2018.03.010. *(Journal article)*

[4]   L. K. Gillespie, "Troubleshooting manufacturing processes" (4th ed.), *Society of manufacturing engineers*, p. 4, ISBN 978-0-87263-326-1. *(Book)*

[5]   S.K. Pradhan, B.B. Nayaka, S.S. Sahayb, B.K. Mishraa, "Mechanical properties of graphite flakes and spherulites measured by nanoindentation", *Carbon,* vol. 47 (2009), pp. 2290 –2299 doi: 10.1016/j.carbon.2009.04.024. *(Journal article)*

[6]   M. N. Bhat, S. Mushtaq, M. Mohbe, "Impact of section thickness on cooling curve morphology, structure and properties of spheroidal graphite cast iron", *Sadhana - Academy Proceedings in Engineering Sciences*, vol. 46, issue 1, December 2021, Article number 17, doi: 10.1007/s12046-020-01541-9. *(Journal article)*

[7]   R.I. El Soeudy, "The effect of graphite aspect ratio on the mechanical and microstructural properties of cast iron", *Materialwissenschaft und Werkstofftechnik*, vol. 33, issue 2, pp. 73 – 79, 2002, doi: 10.1002/1521-4052(200202)33:23.0.CO;2-D. *(Journal article)*

[8]   J. Lu, B. Sun, F. Tang, T. Ding, L. Zhang, "Numerical simulation of temperature field of plasma arc remelting on en-sgj-600-3", *Engineering Review*,vol. 33, issue 2, pp. 115-121, 2013, ISSN 13309587. *(Journal article)*

[9]   L. Collini, A. Pirondi, A. "Fatigue crack growth analysis in porous ductile cast iron Microstructure". *Int. J. Fatigue*. 62/2014, 258–265. http://dx.doi.org/10.1016/j.ijfatigue. 2013.06.020.

[10]   G. Hütter, L. Zybell, M. Kuna, M., "Micromechanisms of fracture in nodular cast iron: From experimental findings towards modeling strategies" – A review. *Eng. Fract. Mech*. 144, 118–141. http://dx.doi.org/10.1016/j.engfracmech.2015.06.042.

[11]   D.O. Fernandino, A.P. Cisilino, R.E. , "Determination of effective elastic properties of ferritic ductile cast iron by computational homogenization, micrographs and microindentation tests. " *Mech. Mater.* 83/2015, 110–121. http://dx.doi.org/10.1016/j.mechmat.2015.01.002.

[12]   W.C. Oliver, G.M., Pharr, "An improved technique for determining hardness and elastic modulus using load and displacement sensing indentation experiments". *Journal of Material Research*, vol. 7, issue 6, p. 1564–1580, ISSN 8842914. *(Journal article)*

[13]   A.C. Fischer-Cripps, "Nanoindentation", *Springer*, 2011, ISBN 978-1-4757-5943-3 *(Book)*

[14]   B. Miao, K. Fang, W. Bian, G. Liu, "On the microstructure of graphite spherulites in cast irons by TEM and HREM", *Acta Metall. Mater.* vol. 38, 1990, pp. 2167–2174, doi: 10.1016/0956-7151(90)90084-T. *(Journal article)*

[15]   J.P. Monchoux, C. Verdu, G. Thollet, R. Fougères, A. Reynaud, "Morphological changes of graphite spheroids during heat treatment of ductile cast irons". *Acta Mater*. vol. 49, 2001, pp. 4355–4362, doi: 10.1016/S1359-6454(01)00230-0. *(Journal article)*

[16]   K. Theuwissen, M. CLafont, L. Laffont, B. Viguier, J. Lacaze, "Microstructural characterization of graphite spheroids in ductile iron". *Trans. Indian Inst. Met.*, vol. 65, 2012, pp. 627–631, doi: 10.1007/s12666-012-0162-5. *(Journal article)*

[17]   C. Bellini, V. Di Cocco, G. Favaro, F. Iacoviello, L. Sorrentino, "Ductile cast irons: Microstructure influence on the fatigue initiation mechanisms". Fatigue Fract Eng Mater Struct. 2019; 42: 2172– 2182. https://doi.org/10.1111/ffe.13100